CHAPTER – 3

Synthesis and Characterization of Zr- or Hf-substituted Magnetite Nanoparticles

3.1 Introduction

As discussed in chapter-1, controlling the therapeutic temperature (42 - 46 °C) is quite challenging during MHT for cancer treatment. This is because of the continuous rise of temperature by MNPS such as pure or substituted magnetite (Fe_3O_4) or maghemite (γ-Fe_2O_3) nanoparticles under ac magnetic field [28,48–52]. It has been stated that a few materials ($ZnGd_xFe_{2-x}O_4$, $Zn_xGd_{1-x}Fe$, $Ni_{1-x}Cr_x$,Cu–Ni alloy and $La_{1-x}Sr_xMnO_3$ nanoparticles) have their T_C near therapeutic temperature [53–55]. But, the low specific magnetization (M_S) and inferior biocompatibility limit their application in MHT. To achieve the desired T_C value, several substituted magnetite (such as Al, Zn, Ni, Mg, Cu, Mn or Co etc.) are prepared [18, 56–59]. However, none of them had their T_C near 50 °C. In contrast, Ti substituted Fe_3O_4 shown comparatively large decreases in the T_C (near ambient temperature) than that of other bivalent and trivalent ions [60].

There are a few studies on tetravalent Zr substituted magnetite [47]. In the recent study, Zr^{4+} ions substituted Fe_3O_4 ($Zr_xFe_{3-x}O_4$, $0 \leq x \leq 1.0$) have displayed significant differences in the properties than that of Ti-substituted Fe_3O_4. This could partially be attributed to the difference in their coordination polyhedral which is ZrO_8 and ZrO_7 for Zr-ions and TiO_6 for Ti-ions. Nevertheless, Hf-ions have HfO_6 types of coordination polyhedral similar to Ti-ions (TiO_6). Thus, the Hf substituted magnetites were expected to behave similar to that of Ti-ions substituted ones. The reports on Hf substituted Fe_3O_4 are though lacking in the literature. Therefore, the present chapter discusses about the effect of substitutions of Zr or Hf on the structural and magnetic properties of Fe_3O_4 nanoparticles. It also discusses about the stabilization of temperature near 42 °C by these MNPs during MHT.

3.2 Zr substituted magnetite nanoparticles

3.2.1 XRD analysis

The XRD patterns (Fig. 3.2.1) demonstrated the single phase of the $Zr_xFe_{3-x}O_4$ ($0.01 \leq x \leq 0.09$) samples having space group Fd3m (JCPDS no. 893854) which were produced by microwave refluxing method. The synthesis procedure of the samples is discussed in chapter-2. However, the structural and magnetic properties for higher concentration of Zr ($0.1 \leq x \leq 1.0$) samples are studied earlier and published by our group [47]. These samples were produced under identical experimental conditions and were found to be monophasic for whole range of substitutions [47]. This study suggests that Fe^{2+}, Fe^{3+} and Zr^{4+} ions get distributed into both the tetrahedral and octahedral voids of Fe_3O_4. Such a distribution of ions was due to the comparable ionic radii of the Fe and Zr – ions (ionic radii for Fe^{2+} and $Fe^{3+}$are 0.77 and 0.63 Å respectively at tetrahedral voids, 0.92 and 0.79 Å at octahedral voids and for Zr^{4+} is 0.72 Å).The occupancy of Zr-ions at both types of voids was facilitated due to ZrO_8 and ZrO_7 type coordination polyhedra in the Zr–O system.

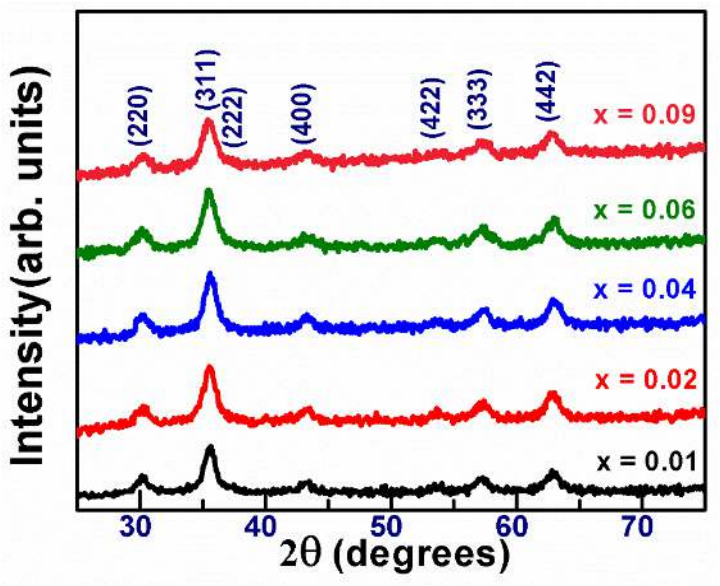

Fig. 3.2.1: XRD patterns for $Zr_xFe_{3-x}O_4$ samples (a) x = 0.01, (b) x = 0.02, (c) x = 0.04, (d) x = 0.06 and (e) x = 0.09 respectively.

3.2.2 TEM analysis

TEM bright field images (fig. 3.2.2) for x = 0.01 and 0.06 samples display the spherical morphology of the particles having size in the range of 5 to 30 nm. The corresponding SAD patterns for the samples were indexed as (2 2 0), (3 1 1), (4 0 0), (3 3 3) and (4 4 0) which further confirms the single phase nature of the samples. Similarly, the samples x = 0.1 and 1.0 also had spherical particles and their size was in the range of 5 – 20 nm [47].

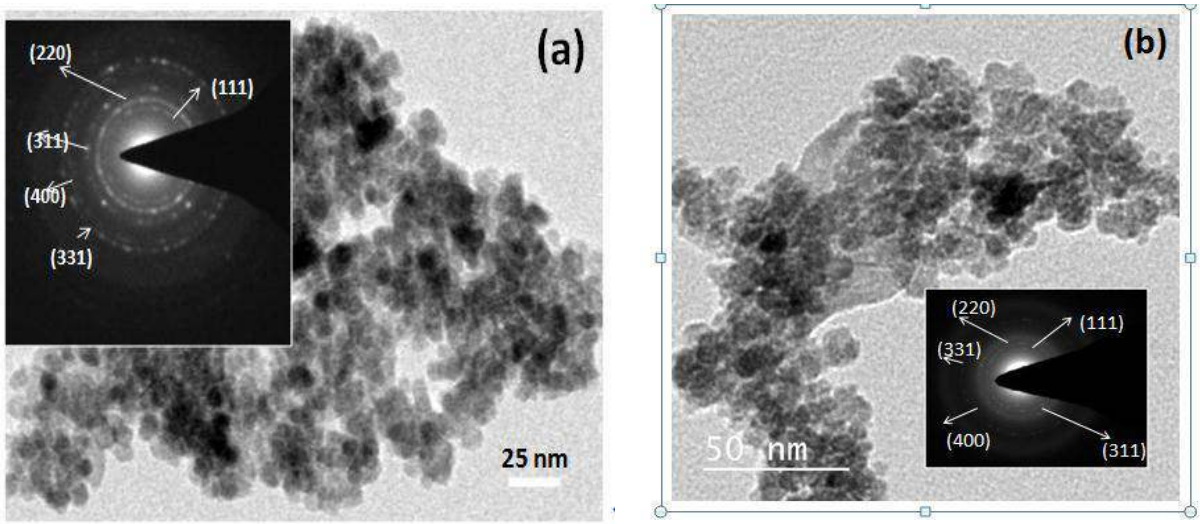

Fig. 3.2.2: TEM micrographs for $Zr_xFe_{3-x}O_4$ samples (a) $x = 0.01$ and (b) $x = 0.06$. The insets show the corresponding SAD patterns for the samples.

3.2.3 Magnetic measurement analysis

The variation of M_S, M_r and H_C obtained from hysteresis loop for $Zr_xFe_{3-x}O_4$ ($0.01 \leq x \leq 1.0$) samples at room temperature and fields up to ± 2 T are shown in Fig. 3.2.3. In this figure, all the values for $x \geq 0.1$ samples were extracted from the reported work for a comparison[47]. The M_S values for these samples were lower than the value for bulk and pure Fe_3O_4 due to submicron sized particles in the present case. Figure 3.2.3 suggests that the M_S value was around 50 Am^2/kg for the samples up to $x = 0.4$. The variation in the M_S values for $x \leq 0.4$ samples can either be attributed to the distribution of Zr^{4+} ions at the two interstitial sites or to a small variation in the particles size [47]. The significant decrease in the M_S values for $x = 0.6$ and 1.0 samples was due to relatively more concentration of Zr^{4+} ions at the octahedral sites [47]. However, the lower M_r and H_C values were attributed to the superparamagnetic nature of MNPs.

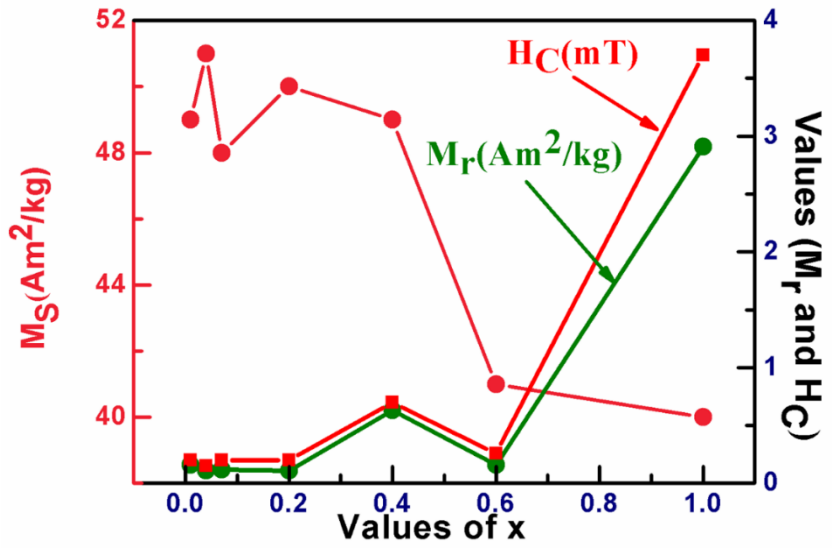

Fig. 3.2.3: The variation of M_S, M_r and H_C for $Zr_xFe_{3-x}O_4$ ($0.01 \leq x \leq 1.0$) samples at room temperature and fields up to ± 2 T.

The magnetization vs. temperature curves were recorded at 50 mT for $Zr_xFe_{3-x}O_4$ ($0.01 \leq x \leq 1.0$) samples (Fig. 3.2.4). The nature of these curves suggests that the T_C value was greater than 300 °C. It has been observed that the substitution of other ions like Mn, Zn, Al, Cu, Cr, Ti in Fe_3O_4 or γ-Fe_2O_3 are found to reduce the T_C value [18, 28, 48–52, 56–59]. Out of these substitutions, the tetravalent Ti-ions was found to be more effective and could reduce nearly to 100 °C [60].

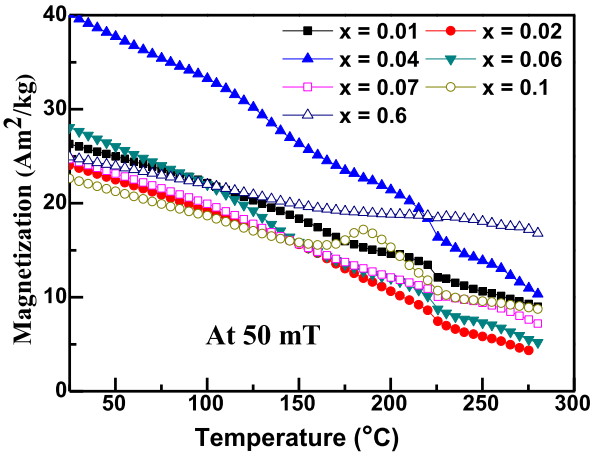

Fig. 3.2.4: The M *vs.* T curves at 50 mT for the $Zr_xFe_{3-x}O_4$ ($0.01 \leq x \leq 0.6$) samples.

3.2.4 Induction heating analysis

The ferrofluids based on $Zr_xFe_{3-x}O_4$ ($0.01 \leq x \leq 1.0$) nanoparticles with a concentration of 40 mg/mL were prepared using oleic acid and water (chapter-2). These ferrofluids were subjected to an AC magnetic field of amplitude 25 mT and frequency 112 kHz. The temperature *vs.* time curves for all the ferrofluids are presented in Fig. 3.2.5. The samples of x = 0.02, 0.04, 0.05, 0.06 and 0.07 exhibit T_S near 43, 47, 55, 37 and 38 °C respectively whereas the other samples (x = 0 and $0.1 \leq x \leq 1.0$) exhibited a continuous rise in temperature (> 60 °C)[47].

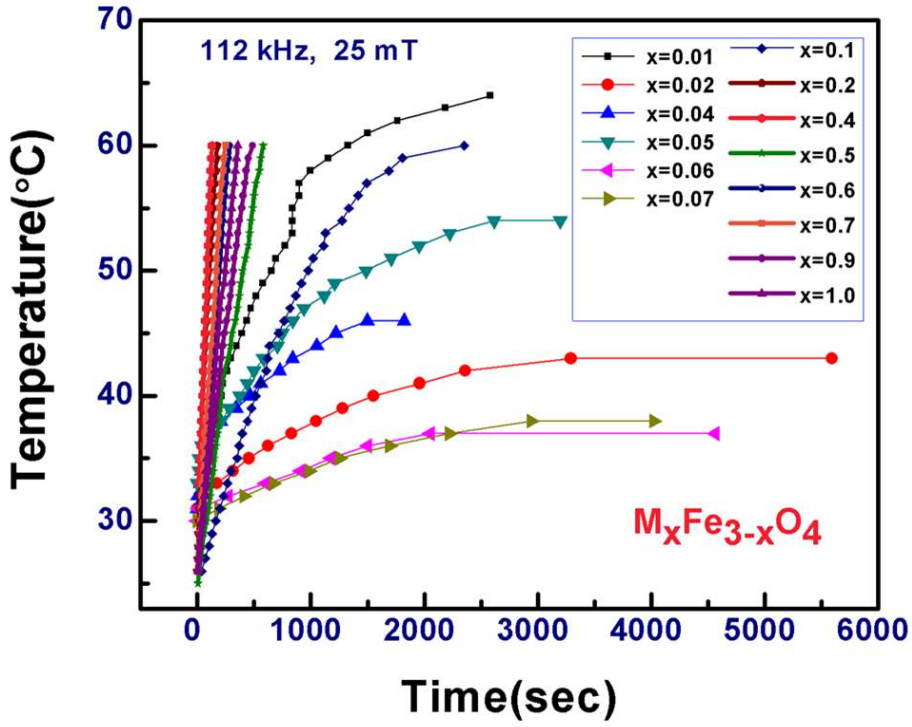

Fig. 3.2.5: The temperature *vs.* time curves for all the ferrofluids based on $Zr_xFe_{3-x}O_4$ ($0.01 \leq x \leq 1.0$) nanoparticles in an AC field with an amplitude of 25 mT and frequency of 112 kHz.

To investigate this aspect further, such experiments at different combinations of fields and frequencies were carried out. For example, in one combination of a field of

amplitude 23 mT and frequency of 173 kHz, the samples with x = 0.6, 0.8 and 0.9 displayed a continuous rise in temperature (Fig. 3.2.6). In contrast, stable temperatures of 29, 33, 31, 39 and 40 °C were observed for the samples with x = 0.04, 0.06, 0.1 0.5 and 1.0 (Fig. 3.2.6). It can be noted that the M_S value for the former samples were relatively smaller than these of the latter one (Fig. 3.2.3). Thus, for some of the samples there was a continuous rise in temperature at one set of field and frequency while they indicated the stability of temperature for another set (Fig. 3.2.6). The temperatures achieved during MHT by different ferrofluids ($Zr_xFe_{3-x}O_4$, $0.01 \leq x \leq 1.0$) at different sets of field and frequencies are displayed in Fig. 3.2.6. To indicate continuous rise in temperature during magnetic hyperthermia for various samples at different sets of field and frequency, the observed temperature was taken at or above 60 °C (Fig. 3.2.6). Other data indicate the T_S values achieved during MHT (Fig. 3.2.6). The same ferrofluid exhibited different T_S value at different sets of fields and frequencies. This is an obvious phenomenon as the heating ability of MNPs is dependent on amplitude of field and frequency. In contrast, there was a continuous rise in the temperature during hyperthermia for Fe_3O_4, γ-Fe_2O_3 and Al-substituted γ-Fe_2O_3 at all sets of fields and frequencies (to be given in Chapter 4) such a phenomenon could be due to the presence of Zr^{4+} ions in the samples or on a combination of field and frequency mentioned earlier.

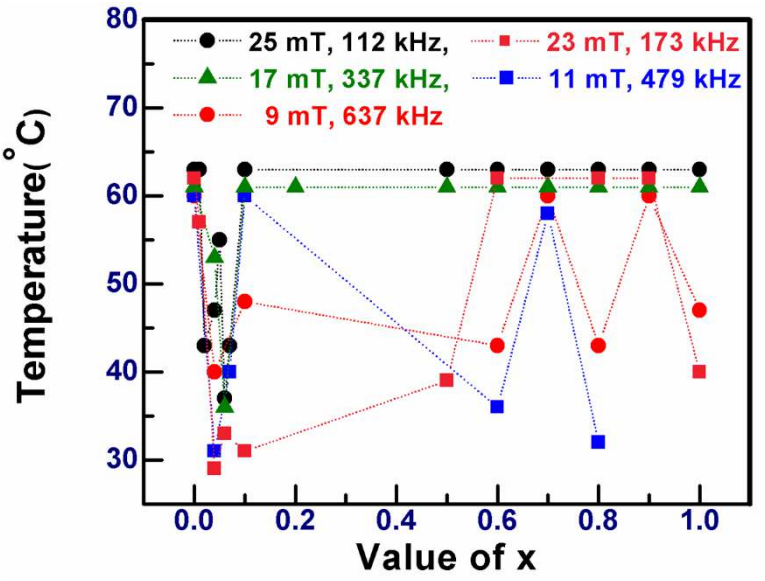

Fig. 3.2.6: The temperatures achieved during MHT vs. Zr concentration at different field strengths and frequencies for $Zr_xFe_{3-x}O_4$, $0.01 \leq x \leq 1.0$ samples.

For more insight into this, hyperthermia experiment was carried out with the fluids of samples x = 0.01 and 0.5 (Fig. 3.2.7) at a field of an amplitude 23 mT and at a frequency 173 kHz having different concentration of MNPs (e.g. 5, 10, 20 and 40 mg/mL). The T_S value at 40 mg/mL concentration for x = 0.01 and 0.5 samples was 56 and 39 °C respectively (Fig. 3.2.7). Further, the T_S value rose to 40, 43 and 58 °C for the concentration 5, 10 and 20 mg/mL of x = 0.01 sample. It suggests that T_S value was proportional to the concentration of MNPs. Such behaviour is also observed by other researchers [35, 40, 42].

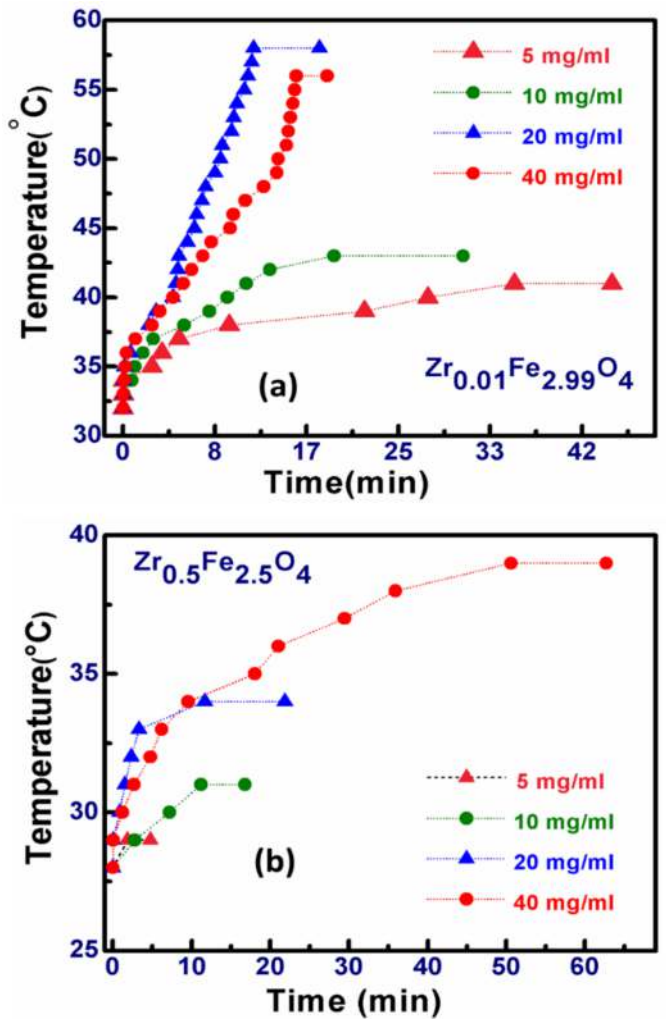

Fig. 3.2.7: The temperature vs. time curve under a field with amplitude of 23 mT and a frequency of 173 kHz with different concentrations of the MNPs (e.g. 5, 10, 20 and 40 mg mL^{-1}) for samples (a) $x = 0.01$ and (b) $x = 0.5$.

The heating rate as well as T_S value for the fluid with a concentration 20 mg/mL was more than that of 40 mg/mL for $x = 0.01$ sample. This could be attributed to the dipolar interactions among the MNPs by which the overall magnetization reduces at higher concentration [61–63]. However, such interaction has negligible role on the T_S value with a concentration 20 and 40 mg/mL. The fluid with MNPs with $x = 0.5$ showed increase in the T_S value with higher concentration of MNPs (Fig. 3.2.7 b).

The dependence of the temperature stability during hyperthermia depending on amplitude and frequency of the magnetic field has not been reported for ferrofluids based on either pure or substituted Fe_3O_4 or γ-Fe_2O_3. Thus, it can be presumed that new emergent magnetic phenomena appear in the presence of tetravalent Zr^{4+} ions in Fe_3O_4 owing to promotion of strong interaction amongst cations. Possibly, Zr^{4+} ions might be influencing Fe^{2+} and Fe^{3+} ions in such a way that for a particular set of amplitude and frequency of the field and at around T_S resultant magnetization dropping in a manner to avoid further rise in temperature. This was even observed for the samples with x = 0.01, which suggests that even a minor addition of Zr-ions (Figs. 3.2.5, 6 and 7) is sufficient to display such behaviour. However, the exact mechanism of stability of temperature during MHT remains unclear.

The SAR values of various samples at different set of field and frequencies are presented in Fig. 3.2.8. It indicates that the SAR values were not showing any particular trend for variation with concentration. This could be attributed to the influence of Zr^{4+} ions on the magnetic properties and hence showed an unprecedented SAR values. In addition, the influence of amplitude and frequencies seems to be useful parameters for the desired SAR values. The SAR values for different concentration of $Zr_{0.5}Fe_{2.5}O_4$ were not estimated as they displayed maximum T_S value below 39 °C. Contrary to this the SAR value was 16.5, 15.9, 6.21 and 2.66 W/g at a concentration of 10, 20 and 40 mg/mL of $Zr_{0.01}Fe_{2.99}O_4$ MNPs.

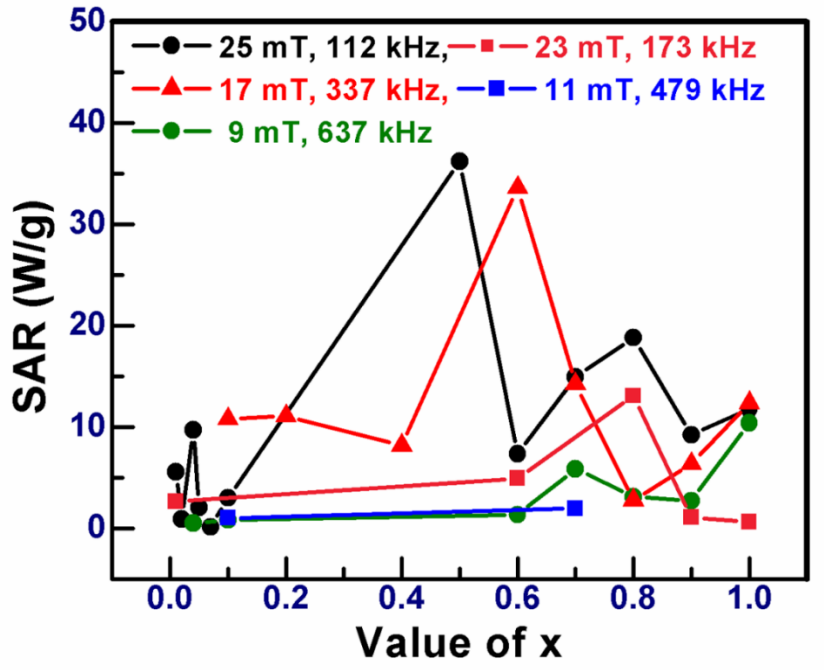

Fig. 3.2.8: The SAR values for the $Zr_xFe_{3-x}O_4$, $0.01 \leq x \leq 1.0$ samples at different field strengths and frequencies.

3.3 Hf substituted magnetite nanoparticles

The stable temperatures during magnetic hyperthermia for Zr^{4+} substituted magnetite samples was thought to be associated with the tetravalent doping. To confirm whether the occurrence of stable temperature depends upon the valence of substituent element, Hf^{4+} substituted Fe_3O_4 nanoparticles were produced by microwave refluxing method (chapter 2). Further, heating ability of these particles were systematically studied. The protocol for the preparation of the ferrofluids for these samples were similar to that of Zr substituted samples.

3.3.1 XRD Study

The X-ray diffraction (XRD) patterns of $Hf_xFe_{3-x}O_4$ (x = 0.01, 0.06, 0.2, 0.4, 0.6 and 0.8) samples are displayed in Fig. 3.3.1. The patterns could be indexed on the basis of

Fe_3O_4 having space group *Fd3m* (JCPDS No. 89-3854). The presence of single phase suggests substitution of Hf^{4+} ions on Fe sites. Such substitutions are possible due to comparative ionic radii of Fe- and Hf-ions. For example the ionic radii of Fe^{2+}, Fe^{3+} and Hf^{4+}ions are 0.77, 0.63 and 0.72 Å respectively at tetrahedral voids while the values reported are 0.92, 0.79 and 0.85 Å, respectively at octahedral voids. Similar substitutions are also reported earlier for Ti- and Zr-ions of the same family [47, 52, 60, 64]. The earlier findings suggest that titanium has TiO_6 coordination whereas zirconium has ZrO_8 and ZrO_7 coordination. Hence the former prefers octahedral void and the latter has preference towards both tetrahedral and octahedral voids[65]. Having HfO_6 co-ordination polyhedra similar to that of titanium, Hf^{4+} ions are expected to occupy mainly at octahedral voids[65]. Nevertheless, the occupancy at tetrahedral voids may not be ruled out completely due to its comparable ionic radius.

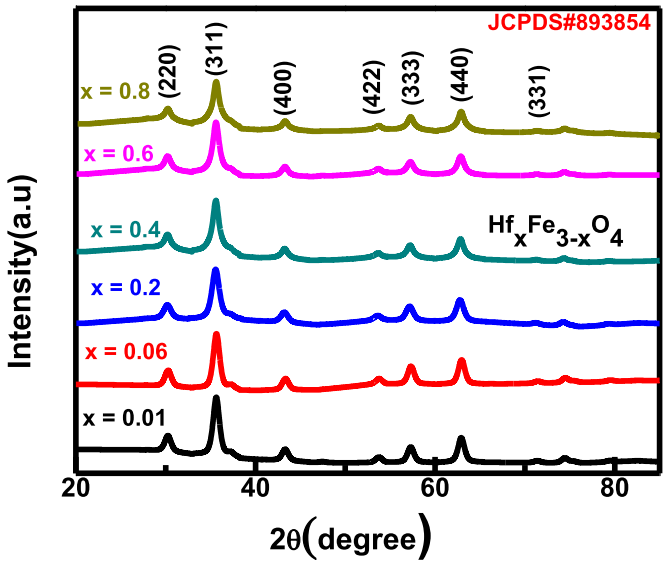

Fig. 3.3.1: XRD patterns of $Hf_xFe_{3-x}O_4$ (x = 0.01, 0.06, 0.2, 0.4, 0.6 and 0.8) samples recorded at room temperature.

A continuous rise in the lattice parameter was observed with increased Hf-concentration in $Hf_xFe_{3-x}O_4$ till $x \leq 0.2$ (Fig. 3.3.2). This could be attributed to Hf^{4+} ions substitution at octahedral sites. With further increase in Hf-substitution, the lattice parameter decreases due to its occupancy at both sites. The average crystallite size for the samples was found to be in the range of 10-16 nm.

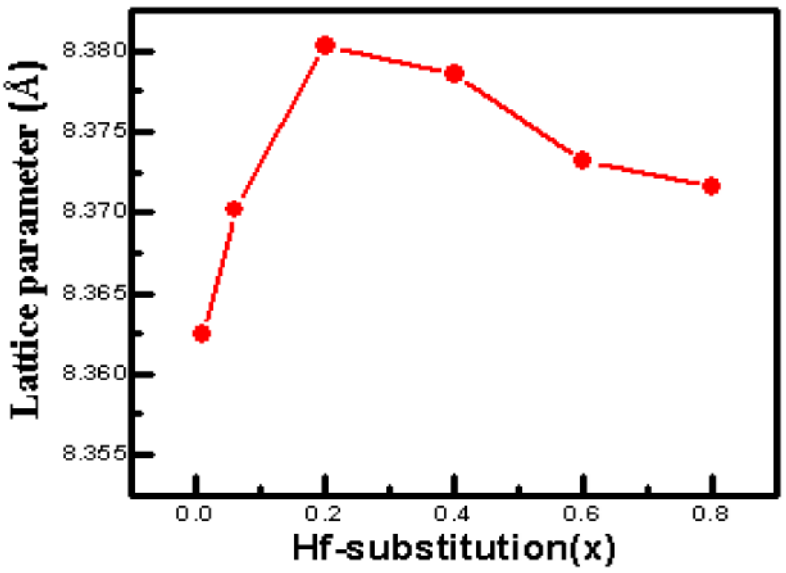

Fig. 3.3.2: Variation in the lattice parameters of $Hf_xFe_{3-x}O_4$ ($0.01 \leq x \leq 0.8$) with Hf-substitution.

3.3.2 TEM-study

The typical TEM bright field image for x = 0.06 and 0.2 samples (Fig. 3.3.3) indicated that the morphology of the particles was spherical shape. The particles size was estimated to be in the range of 10 - 30 nm. The SAD pattern confirms its FCC structure which corroborates the XRD finding.

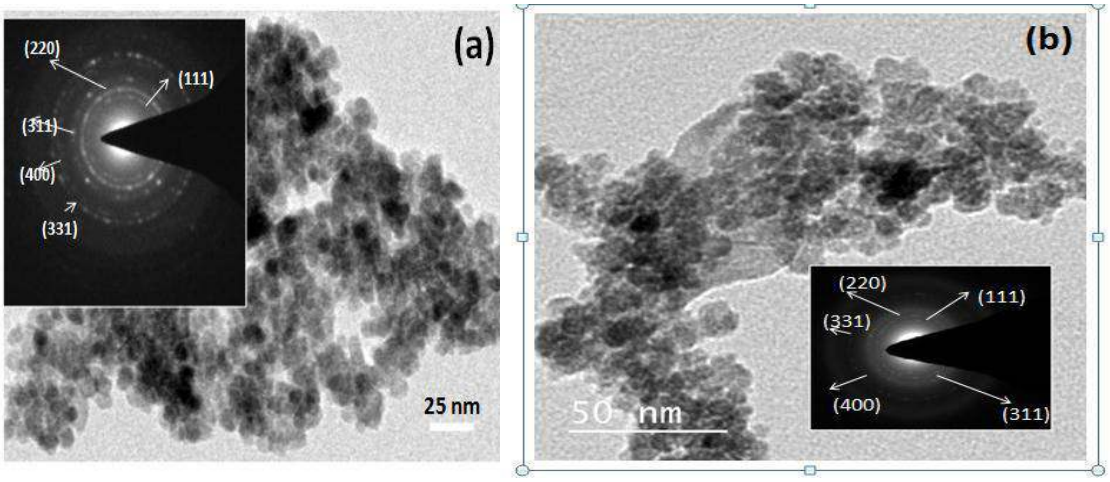

Fig. 3.3.3: TEM micrograph in bright field for a) $Hf_{0.06}Fe_{2.95}O_4$ and b) $Hf_{0.2}Fe_{2.8}O_4$ samples. Inset shows SAD pattern.

3.3.3. XPS study

XPS spectra for $Hf_xFe_{3-x}O_4$ with x = 0.6 and 0.8 compositions are displayed in Fig. 3.3.4. The Fe 2p core level spectrum (Fig. 3.3.4a) exhibits two major peaks at binding energies of 711.3 and 725.8 eV[66]. These peaks correspond to Fe^{3+} $2p_{3/2}$ and $2p_{1/2}$, respectively. In addition to it, peaks at 710.0 correspond to Fe^{2+} $2p_{3/2}$. The Hf 4d core level spectrum exhibits peak at 212.6 eV and it corresponds to Hf^{4+} $4d_{5/2}$ [67]. Fig. 3.3.4c depicts about the formation of two major peaks of Fe 2p at 711.4 and 713.5 eV along with one satellite peak at 725.2 eV for the sample $Hf_{0.8}Fe_{2.2}O_4$. Even Hf 4d fitted

spectrum for this sample shows the peaks at 215.6 and 212 eV correspond to Hf^{4+} $4d_{3/2}$ and $4d_{5/2}$, respectively (Fig. 3.3.4 d). From the analysis of XPS data we can conclude that Fe is in +2 and +3 whereas Hf is in +4 oxidation state only.

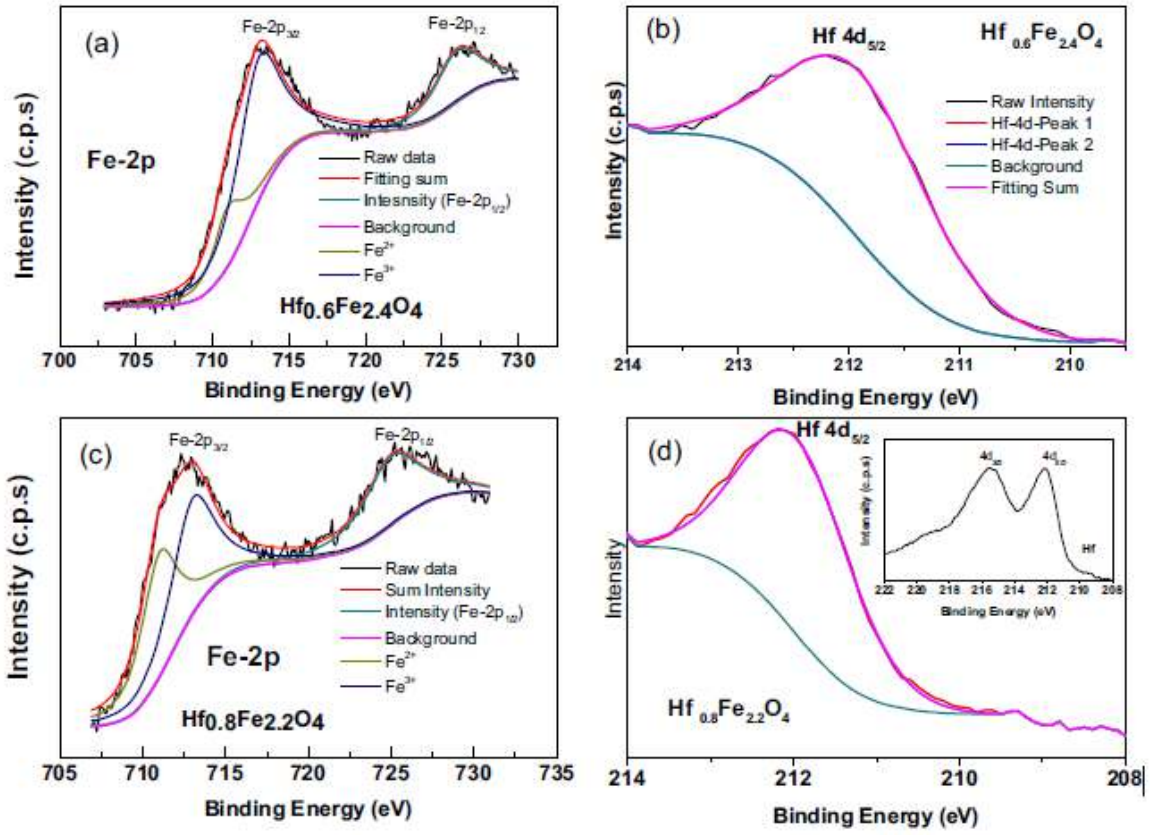

Fig. 3.3.4: XPS spectra for (a) Fe 2p and (b) Hf 4d core level spectra for $Hf_{0.6}Fe_{2.4}O_4$ whereas (c) Fe 2p and (d) Hf 4d core level spectra for $Hf_{0.8}Fe_{2.2}O_4$ sample.

3.3.4. Magnetization study

The room temperature M vs. H curves for as prepared Hf-substituted magnetite (x = 0.01, 0.06, 0.2, 0.4, 0.6, and 0.8) samples are shown in figure 3.3.5. The values of M_S, M_r, and H_C with respect to x are presented in figure 3.3.6. A continuous decrease in the M_S value was observed with increased substitution of Hf^{4+} which suggests that Hf^{4+} get substituted mostly at octahedral sites similar to Ti^{4+} ions [47, 52, 60, 64]. Despite the

preference of Ti^{4+} ions for octahedral site the researchers have also observed its occupancy at tetrahedral voids at higher concentration.

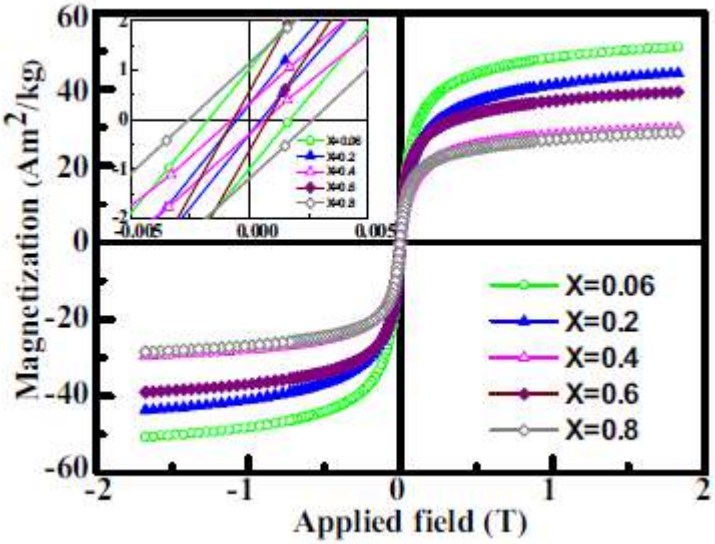

Fig. 3.3.5: M vs. H curves for $Hf_xFe_{3-x}O_4$ ($0.06 \leq x \leq 0.8$) samples at 300 K and ±1.8 T.

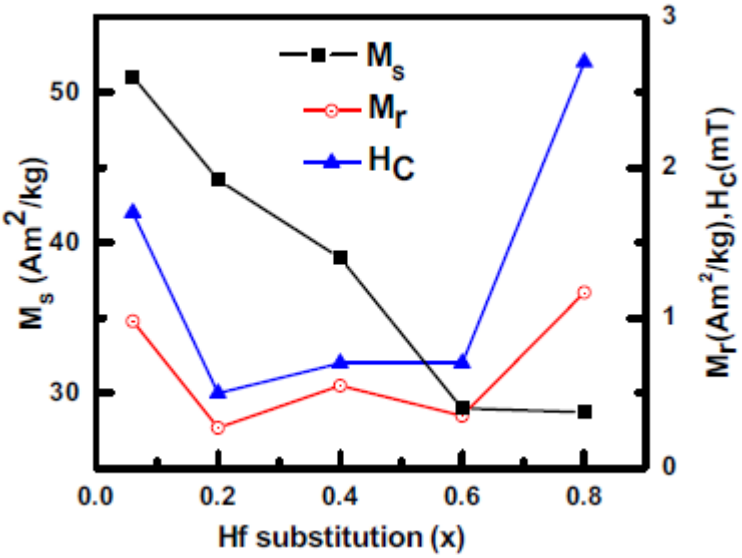

Fig. 3.3.6: Variation of M_S, M_r and H_C values with Hf concentration for $Hf_xFe_{3-x}O_4$($0.01 \leq x \leq 0.8$) samples.

Similarly, at higher concentrations, Hf^{4+} ions may have also occupied at tetrahedral voids. From the magnetization data (figure 3.3.5), the one of the possible distribution of Fe^{2+}, Fe^{3+} and Hf^{4+} ions at tetrahedral and octahedral sites can be given as follows:

$$(Fe^{3+})_A[Fe^{3+}_{1-2x}Fe^{2+}_{1+x}Hf^{4+}_x]_BO_4 \text{ for } x \leq 0.2,$$

$$(Fe^{3+}_{0.8}Fe^{2+}_{0.1}Hf_{0.1}{}^{4+})[Fe^{3+}_{0.4}Fe^{2+}_{1.3}Hf_{0.3}{}^{4+}] \text{ for } x = 0.4,$$

$$(Fe^{3+}_{0.68}Fe^{2+}_{0.16}Hf_{0.16}{}^{4+})[Fe^{3+}_{0.12}Fe^{2+}_{1.44}Hf_{0.44}{}^{4+}] \text{ for } x = 0.6 \text{ and}$$

$$(Fe^{3+}_{0.6}Fe^{2+}_{0.3}Hf_{0.3}{}^{4+})[Fe^{2+}_{1.5}Hf_{0.5}{}^{4+}] \text{ for } x = 0.8$$

From the ionic distributions the estimated resultant magnetization as 3.94, 3.64, 2.8, 2.5, 2.32 and 2.8 μ_B per ions for samples with x = 0.01, 0.06, 0.2, 0.4, 0.6 and 0.8 respectively. The experimental values for M_S were smaller than that of theoretical values which could be due to the presence of submicron sized particles. However, the decreasing trend in the M_S values with increased Hf concentration for experimental values were similar to that of calculated values (Fig. 3.3.6). Though the theoretical value of M_S for x = 0.8 was more than x = 0.6 sample but experimental values were almost same (Fig. 3.3.6).

The values of M_r and H_C suggest that the samples were close to superparamagnetic nature (Fig. 3.3.6). For the samples x = 0.8, the M_r and H_C value was bit higher which could be attributed to the presence of large amount of nonmagnetic Hf^{4+} ions. The magnetization *vs.* temperature curves for the sample with x = 0.05, 0.2 and 0.8 at 10 mT are shown in Fig. 3.3.7. It can be inferred that the T_C values for the samples was higher than 325 °C. The rise in the magnetization value near 225 °C could be attributed to the possible grain growth of nanosized particles.

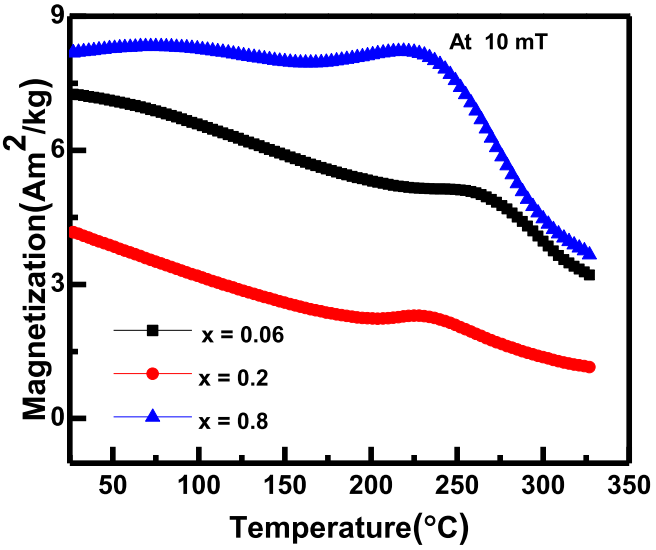

Fig. 3.3.7: Magnetization *vs.* Temperature curves (field cooled data) for $Hf_xFe_{3-x}O_4$ (for x = 0.06, 0.2 and 0.8) at 10 mT.

3.3.5. Mössbauer spectroscopy study

The Mössbauer spectra recorded at room temperature for composition x = 0.06, 0.4 and 0.8 samples are presented in Fig. 3.3.8. The values for hyperfine field (B_{Hf}), isomer shift (IS), quadruple splitting (QS) line width, relative area (R_A%) and fitting quality of different Fe sites are summarized in table 3.3.2. The Mössbauer spectra of $Hf_{0.06}Fe_{2.94}O_4$ sample could be fitted with three sextets (six lines Zeeman splitting patterns). Out of these, sextet A (with higher B_{hf} value) was identified for Fe^{3+} ions at tetrahedral site whereas the sextet B (with lower B_{hf} value) could be acknowledged for Fe^{2+} and Fe^{3+} ions at octahedral site of inverse spinel structure. The third sextet C indicates for Fe^{3+} ions that have shorter spin relaxation time due to the superparamagnetic nature of the nanoparticles. The B_{Hf} values were relatively lower than the bulk value which can be corroborated to the submicron sized particles (table 3.32). However, more

decrease in the hyperfine field at octahedral site could be attributed to relatively more doping of Hf-ions at this site (Fig. 3.3.9 a). This observation was consistent with XRD and magnetic properties findings. The samples with x = 0.4 and 0.6 were fitted with two sextets and a doublet (Fig. 3.3.8). Similar to other sample, the sextets with higher B_{hf} values represents tetrahedral site whereas with lower values indicate octahedral site.

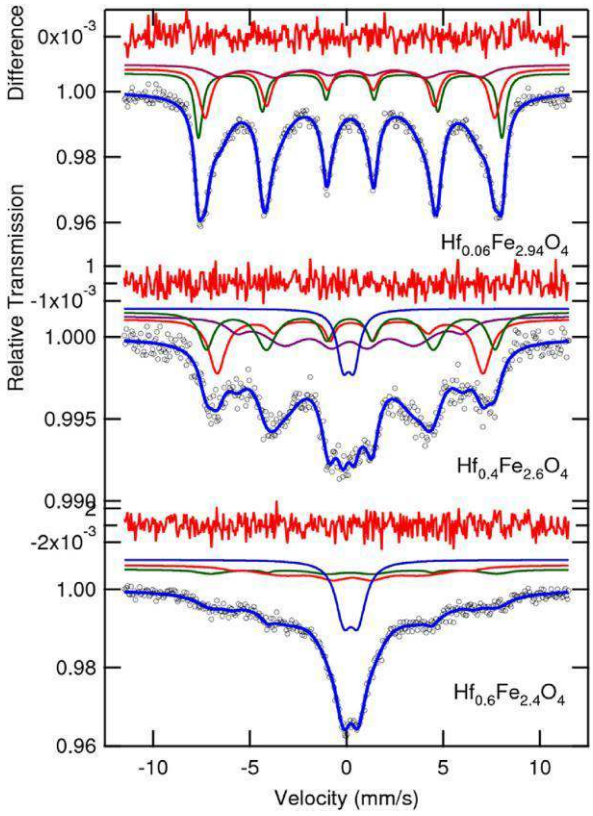

Fig. 3.3.8: Room temperature Mössbauer spectra for $Hf_xFe_{3-x}O_4$(x = 0.06, 0.4 and 0.6) samples.

A continuous decrease in the B_{HF} values were observed for both tetrahedral and octahedral sites with increased Hf-concentrations. Nevertheless the decrease was much steeper for octahedral sites. This strengthens our findings that Hf prefers octahedral site (HfO_6 polyhedra) however it also occupies tetrahedral site at higher concentration. There

were doublets for both the samples which correspond to superparamagnetic component in the samples due to submicron sized particles. The presence of doublet are attributed to lower value of relaxation time (τ) than 10^{-9} s or than τ_L (Larmor precession time)[64]. The paramagnetic component has increased with increased Hf concentration due to its nonmagnetic nature.

Table 3.3.2:The values of hyperfine field (BHF), isomer shift (δ), quadrupole splitting (Δ), linewidth (Γ) and relative areas (R_A) in percentage of tetrahedral A(Fe^{3+}) and octahedral B sites of (Fe^{3+}, Fe^{2+}) ions for $Hf_xFe_{3-x}O_4$ (x = 0.06, 0.4 and 0.6) samples derived from Mössbauer spectra recorded at room temperature.

Sample Comp. (x)	**Iron Sites**	**Hyper. field, (H_{hf}) Tesla (±0.2)**	**Quadrupole splitting, (Δ) mm/s (±0.01)**	**Isomer shift (δ) mm/s (±0.01)**	**Line width (Γ) mm/s (±0.1)**	**Area (R_A) %**	**Fitting quality (χ^2)**
0.06	Sextet A (Fe^{3+})	48.7	0.005	0.302	0.432	20.4	1.08515
	Sextet B (Fe^{3+}, Fe^{2+})	46.5	-0.029	0.301	0.568	29.8	
	Sextet C (Fe^{3+})	41.8	-0.022	0.299	1.324	49.8	
0.4	Sextet A (Fe^{3+}, Fe^{2+})	46.3	0.033	0.322	0.474	21.0	0.9838
	Sextet B (Fe^{3+},Fe^{2+})	42.7	-0.048	0.342	0.596	15.3	
	Sextet C (Fe^{3+})	36.3	0.033	0.291	1.736	59.9	
	Doublet (Fe^{3+})	--	0.577	0.248	0.733	3.8	
0.6	Sextet A (Fe^{3+},Fe^{2+})	45.8	0.193	0.377	1.86	18.6	0.9896
	Sextet B (Fe^{3+}, Fe^{2+})	38.8	0.006	0.416	1.915	65.7	
	Doublet(Fe^{3+})	--	0.742	0.334	0.975	15.7	

Sextet A: Tetrahedral A-site, Sextet B – Octahedral B site, sextet C: Relaxation effect.

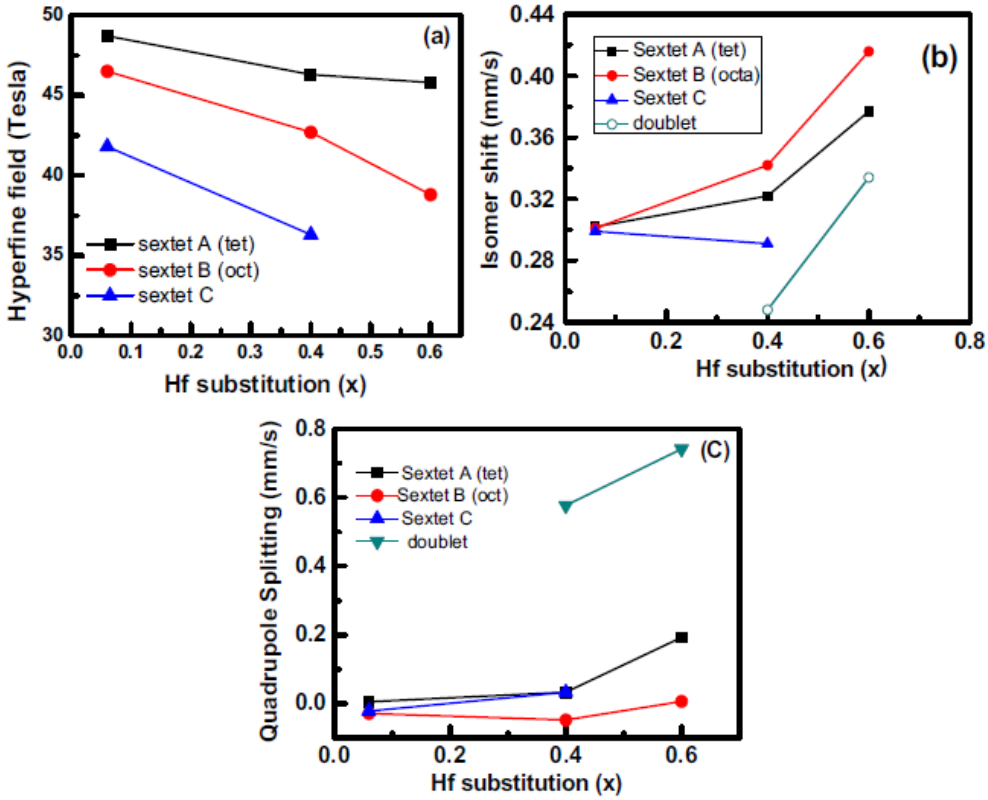

Fig. 3.3.9: Variation in (a) hyperfine field (BHF), (b) isomer shift (d), and (c) quadrupole splitting (D) with Hf substitutions in $Hf_xFe_{3-x}O_4$samples (for x = 0.06, 0.4 and 0.6).

A continuous rise in the *IS* values for both tetrahedral and octahedral sites with increased Hf-concentrations (Fig. 3.3.9b), also confirms the preferential occupancy of Hf-ions in the spinel structure at both the sites. The relatively more increase in this value at octahedral site for x = 0.6 sample further confirmed more Hf occupancy at octahedral site. As discussed earlier, each Hf^{4+} ion substitution causes replacement of one Fe^{3+} ion and simultaneous reduction of another Fe^{3+} ion into Fe^{2+} ions to maintain the charge neutrality. Therefore the IS values for both the sites increase with increased Hf concentration (Fig. 3.3.9b). The variation of Quadrupole splitting with Hf substitution is also presented in Fig. 3.3.9c. The values were quite less for the sextets than that of doublets this is due to the presence of MNPs having superparamagnetic nature[68,69].

3.3.6 Induction heating analysis

The temperature *vs.* time curves were recorded for the magnetic fluids prepared using $Hf_xFe_{3-x}O_4$ ($0.06 \leq x \leq 0.8$) samples in an AC magnetic field of amplitude 23 mT and of frequency 173 kHz (Fig.3.3.10). For all the ferrofluids, the concentration of the MNPs was 40 mg/ mL. At same concentration, for $x = 0$ i.e. pure Fe_3O_4 sample, the heating rate was too fast to note down the time for individual temperature rise (not given in the figure). For the samples with $x = 0.06$, 0.08, 0.2 and 0.4, T_S values were observed during MHT. The T_S value was 38, 33, 52 and 40 °C, respectively for the samples with $x = 0.06$, 0.08, 0.2 and 0.4, respectively (Fig. 3.3.10). In contrast, there was a continuous rise in temperature even beyond 60 °C for the fluids of the samples with $x = 0.6$ and 0.8 respectively (Fig. 3.3.10). This happened despite the former samples had better magnetization than the latter ones (Fig. 3.3.6). The stabilization of temperature during MHT generally occurs near T_C for ferromagnetic and ferrimagnetic materials as they transform to paramagnets. However the T_C value for the samples was well above 325 °C (Fig. 3.3.7).

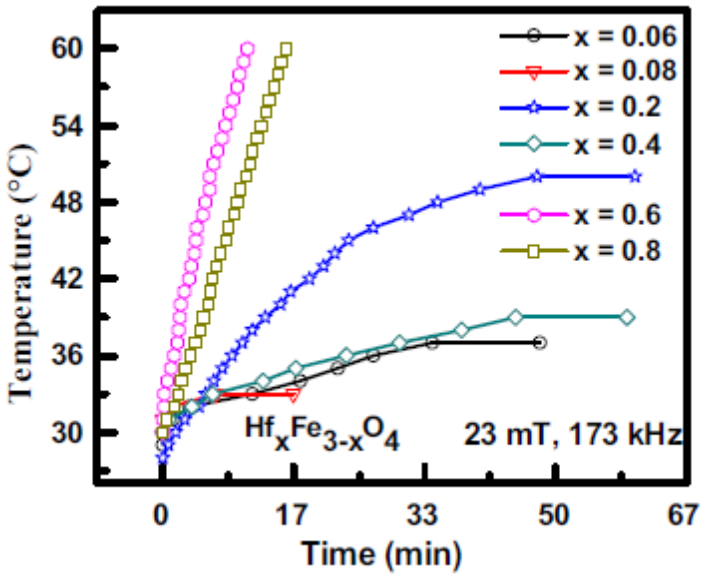

Fig. 3.3.10: Temperature *vs.* time curves for $Hf_xFe_{3-x}O_4$ ($0.06 \leq x \leq 0.8$) samples at a Field of amplitude 23 mT and a frequency 173 kHz.

Similar experiment was then carried out in a field of amplitude 17 mT and a frequency of 337 kHz. At this field, the samples with x = 0.08, 0.2, 0.4, 0.6 and 0.8 displayed a continuous rise in temperature whereas the sample with x = 0.06 show T_S value near 50 °C (Fig. 3.3.11). The obtained values of T_S for different concentrations of Hf in Fe_3O_4 at various fields are depicted in Fig. 3.3.11. The T_S values at or above 60 °C indicate a continuous rise in temperature during MHT. The value of T_S was found to be different for the same sample at different fields. Even it was not a direct function of the strength of the field and frequency combinations (Fig. 3.3.11). The observed stabilization of temperature during MHT was due to the presence of tetravalent Hf^{4+} ions in the samples. As mentioned earlier, the stabilization temperature was also observed for Zr^{4+} ions substituted samples. Hence, tetravalent ions might have introduced some kinds of magnetic phenomena in the system which brought a halt in the temperature rise during hyperthermia. This might be either due to transformation of ferromagnetic phase into paramagnetic phase which was purely dependent of amplitude and frequency of ac magnetic field. Otherwise, it could be due to transformation of ferrimagnetic phase into antiferromagnetic, that was again based on the strength of magnetic field. The different T_S values for the same sample at different fields also support the crucial role of magnetic field on the observed phenomena (Fig. 3.3.11). Though unknown phenomenon but role of temperature achieved during experiment might have also be a parameter for this behaviour.

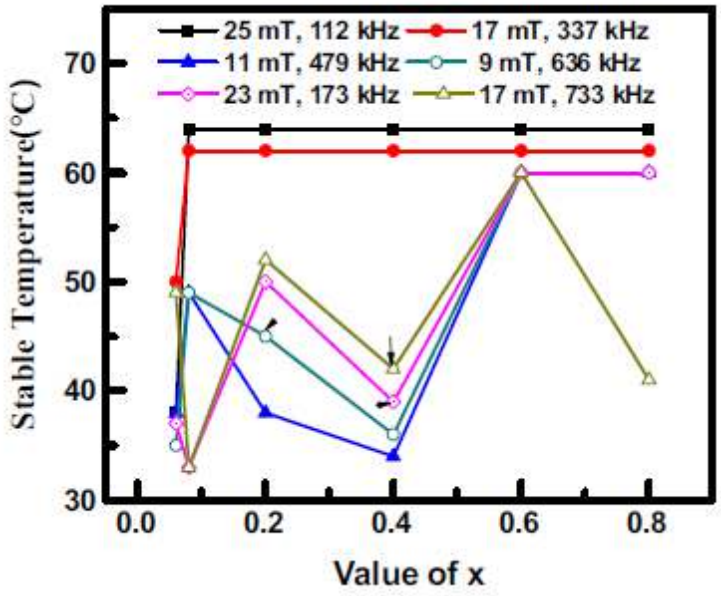

Fig. 3.3.11: Stable temperature vs. Hf-concentration plot for $Hf_xFe_{3-x}O_4$ ($0.01 \leq x \leq 0.8$) samples at different Field and frequency. Points lying in 42 - 46 °C are indicated by arrow for clarity.

The SAR values for $Hf_xFe_{3-x}O_4$ ($0.01< x \leq 0.8$) based fluids at different frequency and field are given in figure 3.3.12. Like T_S values, the SAR values were also found to be a function of amplitude and frequency of the fields. Though, the heating rate for the samples is comparable to the earlier results but the SAR values were relatively low[42, 52, 70, 71]. This could be attributed to the dependence of SAR values on the parameters like almost type, size, shape, polydispersity of the MNPs, physical and chemical properties of the carrier fluid, coating materials, amplitude and frequency of magnetic field and whether it is calculated with respect to per g of Fe or Fe-oxides [42, 52, 70, 71].

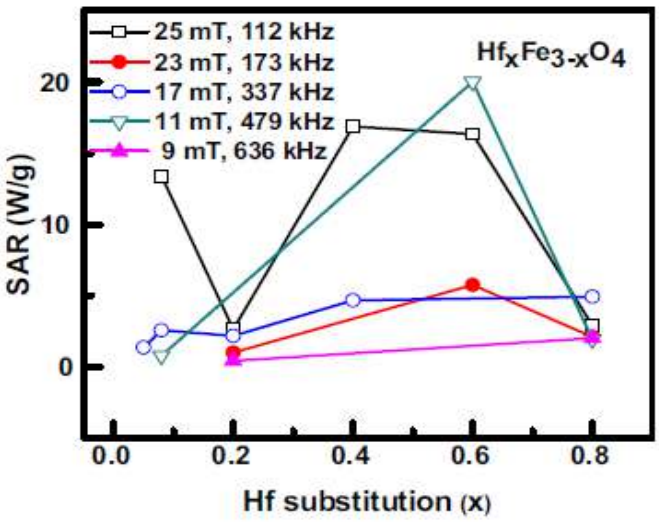

Fig. 3.3.12: The SAR values vs. Hf substitution for $Hf_xFe_{3-x}O_4$ ($0.01< x \leq 0.8$) samples at different frequencies and fields.

3.4 Conclusions

The nanoparticles of $Zr_xFe_{3-x}O_4$ ($0.01 \leq x \leq 1.0$) and $Hf_xFe_{3-x}O_4$ ($0.01< x \leq 0.8$) were produced by microwave refluxing method. The substitutions of Zr or Hf-ions over the whole range were confirmed by XRD and TEM analyses. The M_S value was continuously varying with respect to Zr substitutions. This is due to the substitutions of Zr^{4+} ions in both tetrahedral and octahedral sites. On the other hand, the M_S value was 51.07 Am^2/kg for x = 0.06 for $Hf_xFe_{3-x}O_4$ sample which decreased continuously with increased substitutions. The preferred substitutions of Hf-ions are at octahedral sites at lower concentrations. It however does go to tetrahedral sites at higher concentration. This was confirmed by XRD, Mössbauer spectra and magnetization results. The ferrofluids of the single phase $M_xFe_{3-x}O_4$ ($0.01 \leq x \leq 1.0$, M = Zr or Hf) system displayed temperature stability (T_S~ 42–46 °C) during hyperthermia at a suitable combination of frequency and amplitude of the field strength.